Performance analysis of an all-dielectric planar Mikaelian lens antenna for 1-D beam-steering application

WENYI SHAO[*] AND QIANG CHEN

Department of Communications Engineering, School of Engineering, Tohoku University, Sendai 980-8579, Japan
[*]*wenyi.shao.s1@dc.tohoku.ac.jp*

Abstract: This paper investigates the performance of an all-dielectric planar Mikaelian lens based on ray transfer matrices and full-wave analysis for 1-D beam-steering application. This new lens concept has its intrinsic flat shape characteristic allowing for a simple low-cost planar feed technology. To verify the design concept, a lens prototype excited by five rectangular microstrip patch antennas with perforated structure (21×24 holes) is fabricated using stereolithography (SLA) 3-D printing. The simulated and measured results of the proposed lens prototype, operating at 10 GHz, shows that the switched-beam coverage over a certain range of beam-steering angles can be obtained. The intrinsic phase error of lens resulting from comatic aberration exhibits obvious increase as the off-axis angle of beam increases, which leads to further deterioration of the corresponding radiated beam. The beam-steering capabilities from −20° to +20° with around 13.2 dBi of realized gain and side-lobe level (less than −11.5dB), and up to potential steering angles (±30°) with around 10 dBi of realized gain can be steadily achieved. Moreover, the realized gain, efficiency and side-lobe level can be further improved to get better radiation performances by using other materials with lower loss tangent. Due to its intrinsic flat shape characteristic, this lens concept could be a potential alternative to develop a low-cost, low-profile and easy-to-fabricate beam-switching array antenna for microwave communication applications.

1. Introduction

Beam-steering antennas have played an essential role in next generation wireless communications (5G) systems for high data-rate, flexible coverage capability and multipoint communications [1]. Traditionally, three main and popular configurations for beam-steering have been put forth namely electronically phased array antennas (EPAA), mechanically steerable reflector antenna (MSRA) and lens antenna. Although the beams with high gain can be quickly steered across a certain angular scope, the EPAA requires masses of active antenna modules and phase shifters to be active simultaneously for electronic beam steering [2], making the EPPAA high cost. Additionally, these large-scale antenna modules and phase shifters consume significant amount of electrical power. On the other hand, steerable beams can be simply obtained by using mechanical moving or rotating device to change the reflector antenna toward the desired direction or move the source feed along the focal plane [3]. Nevertheless, the MSRA makes the overall systems bulky and vulnerable to interference due to its physical dimensions constraint and the feed blockage. Similar to the reflector antenna, the beam-steering capability of traditional lens antenna is also limited especially for the off-axis steering. Although their high efficiency and large bandwidth in very wide-angle region [4], traditional lens are usually cumbersome and high profile.

Compare to the EPAA, MSRA and traditional lens antenna, gradient index (GRIN) lens antenna can flexibly achieve wide beam-steering angles with competitive efficiency, broadband and less deterioration of the beam, which has received significant attention in recent years. There have been several well-known GRIN lenses, such as Luneburg lens [5,6], Maxwell fisheye

lens [7,8], Gutman lens [9] and Eaton lens [10]. Although these GRIN lenses have various refractive index distributions, a common feature among them is the spherical characteristic of their shapes that poses a challenge for fabricating and integrating the standard planar feed sources such as waveguides and patch antenna arrays to the lens's surface. To eliminate the limitation of its spherical or hemispherical shape, additional complex approaches such as transformation optics (TO) [6] and quasi-conformal transformation optics (QCTO) [11] are required to modify the profile of the refractive index. Besides, these conformal mapping transformations lead to a reduction of beam-steering angle range [12]. Unlike these GRIN sphere lenses, Mikaelian lens, also called hyperbolic cosine lens or hyperbolic secant lens, has a unique intrinsic flat shape characteristic, which has attracted a lot of interest in the application field of microwave and millimeter wave [13–17] in recent years. Due to the cylindrical symmetry of its refractive index distribution, Mikaelian lens can be easily fabricated. However, all these previous studies are mainly focused on the focusing properties analysis that the suitable feeding source can be placed at the focal point of lens to achieve good radiation performance. As one of the most fundamental and important properties, the beam-steering capability of Mikaelian lens has not been investigated in the literature of microwave or millimeter wave applications. Besides, the GRIN lens presenting desired graded permittivity profile can be manufactured by metamaterials, foam and ceramic materials, which requires the complicated, expensive and special process techniques. Compared to the dielectric structures, metamaterials consisting of sub-wavelength metallic resonant structures have also the inherent drawbacks of large loss and narrow bandwidth. However, the perforated dielectric material structures avoid using metal structure can be easily and quickly fabricated by easily accessible 3-D printing technique at a low-cost.

In this paper, to the best of our knowledge, the capability of beam-steering for an all-dielectric planar Mikaelian lens is first explored based on ray transfer matrices and full-wave analysis. The proposed lens prototype excited by five rectangular microstrip patch has been evaluated at 10 GHz. These patch antennas are placed at the focal plane of lens to obtain switched-beam coverage over a certain range of beam-steering angles. Benefiting from the 3-D printing technique, the proposed lens can be easily fabricated, which provides a potential alternative to develop a low-cost, low-profile and easy-to-fabricate beam-switching array antenna for microwave communication applications.

2. 1-D Beam steerable Mikaelian lens antenna design

### 2.1. Design theory of Mikaelian lens using ray transfer matrices

Mikaelian lens has unique characteristics of self-focusing that the rays oscillate in a sinusoidal way along the optical axis (z-axis) [18] as shown in Fig. 1(a). The oscillation period of the rays inside lens is defined as pitch (p). Both the pitch and width (w) of lens can be also easily adjusted to achieve the focusing phenomenon on the lens surface as illustrated in Fig. 1(b). Hence, it provides a potential way to apply this lens concept to design integrated lens antennas configurations by just selecting the appropriate the pitch and width of lens.

The transverse refractive index profile of Mikaelian lens varies with radial direction (x) as defined in the following equation.

$$n(x) = n_0 \text{sech}\left(\frac{2\pi px}{w}\right), \tag{1}$$

where n_0 is the central refractive index along z-axis.

It is well known that the ray tracing theory is a very useful tool to deal with the electromagnetic wave propagation in GRIN lens. The ray equation can be mathematically determined by the
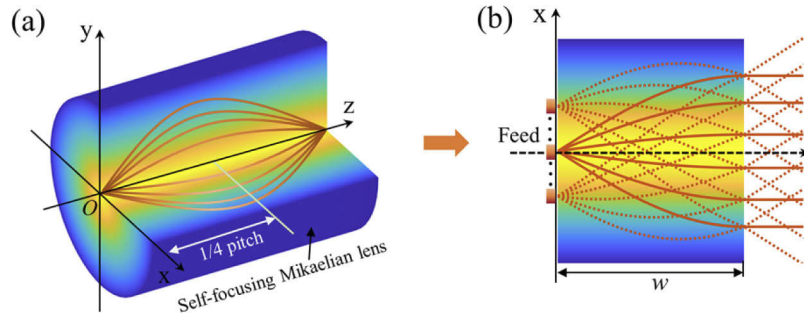
Fig. 1. The unique self-focusing properties of Mikaelian lens. (a) The rays oscillate in a sinusoidal way along the optical axis inside lens. (b) Schematic of integrated lens antennas configurations with appropriate the pitch and width.

following equation.

$$\frac{d}{ds}\left[n\frac{dr}{ds}\right] = \nabla n, \tag{2}$$

where r is the vector form of position (x, z), and $ds = \sqrt{dx^2 + dz^2}$ is the differential arc length along the ray trajectory.

Here, we define $\dot{x} = dx/dz$. The ray propagation inside lens can be further described by 2-by-2 ray transfer (ABCD) matrices. In other words, the distance (x_i) from the optical axis (z-axis) and by the slope $(\dot{x}_i)$ in any plane perpendicular to z-axis can be used to describe the ray trajectory. i represents the different points along ray trajectory. Let us first consider the generalized propagation form of a ray from air into lens and back into air, as shown in Fig. 2(a). The ray propagates in the xoz plane, and the z-axis is the optical axis.
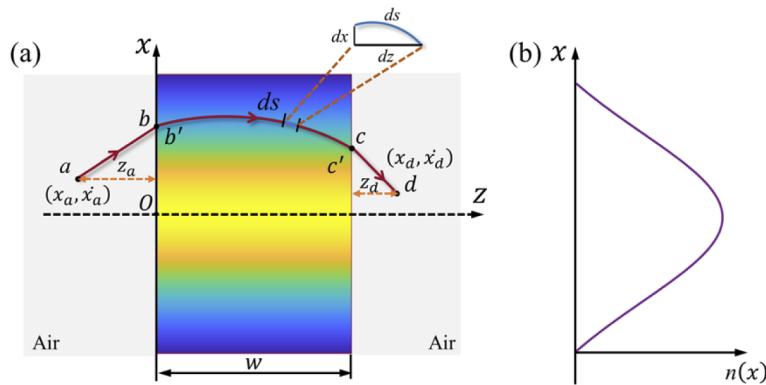
Fig. 2. (a). The generalized propagation form of a ray from air into lens and back into air. (b). The transverse refractive index profile of lens.

Under the paraxial approximation, the 2-by-2 ray transfer (ABCD) matrices can be written as follows (details of the derivation can be seen in [17])

$$\begin{pmatrix} A & B \\ C & D \end{pmatrix} = \begin{pmatrix} 1 & z_d \\ 0 & 1 \end{pmatrix} \cdot \begin{pmatrix} 1 & 0 \\ 0 & n_0/n_{air} \end{pmatrix}$$
$$\begin{pmatrix} \cos(\alpha z) & \sin(\alpha z)/\alpha \\ -\alpha\sin(\alpha z) & \cos(\alpha z) \end{pmatrix} \cdot \begin{pmatrix} 1 & 0 \\ 0 & n_{air}/n_0 \end{pmatrix} \cdot \begin{pmatrix} 1 & z_a \\ 0 & 1 \end{pmatrix}, \tag{3}$$

where $\alpha = 2\pi p/w$ is the gradient parameter of lens.

After performing matrix operations, we can obtain the corresponding parameters from Eq. (3) respectively.

$$
\begin{cases}
A = \cos(\alpha z) - \alpha n_0 z_d \sin(\alpha z) \\
B = z_a \cos(\alpha z) - \alpha n_0 z_a z_d \sin(az) + \frac{1}{n_0 \alpha} \sin(az) + z_d \cos(\alpha z) \\
C = -n_0 \alpha \sin(\alpha z) \\
D = -n_0 \alpha z_a \sin(\alpha z) + \cos(\alpha z)
\end{cases}
. \tag{4}
$$

The ray trajectory from a point a to d can be determined as follows.

$$
\begin{pmatrix} x_d \\ \dot{x}_d \end{pmatrix} = \begin{pmatrix} A & B \\ C & D \end{pmatrix} \begin{pmatrix} x_a \\ \dot{x}_a \end{pmatrix} = \begin{pmatrix} A x_a + B \dot{x}_a \\ C x_a + D \dot{x}_a \end{pmatrix}. \tag{5}
$$

Then, substituting (1) and (4) into (5), we can obtain the ray position (x_d) and slope ($\dot{x}_d$) in a general form respectively.

2.2. Structure realization of proposed Mikaelian Lens

Traditionally, metamaterials [9] consisting of metallic resonant structures, porous foam [13], dielectric material with air-hole structure [17] and ceramic materials [19] are utilized to achieve intended permittivity profile with different manufacturing techniques. Benefiting from the 3-D printing technology, the proposed all-dielectric lens with air-hole structure can be easily fabricated at a low-cost.

Figure 3 illustrates the implemented design the procedure of Mikaelian lens operating at 10 GHz. Using staircase approximation, the continuous relative permittivity profile of lens as shown in Fig. 3(a) is discretized into 24 layers. In order to achieve the desired discrete relative permittivity distribution, the different sizes of perforation are utilized for simplicity based on the effective medium theory as shown in Fig. 3(c). The dielectric constant of the material used for manufacturing is about 2.8. Considering that the SLA 3D printing is more accurate than FDM (fused deposition modeling), the perforation structure (21×24 holes) of lens in our case is fabricate by using SLA 3-D printing. The air hole sizes for different layers of lens are listed in Table 1. It is noted that only half of layers is shown in Table 1 owing to the axial symmetry of relative permittivity profile of lens.
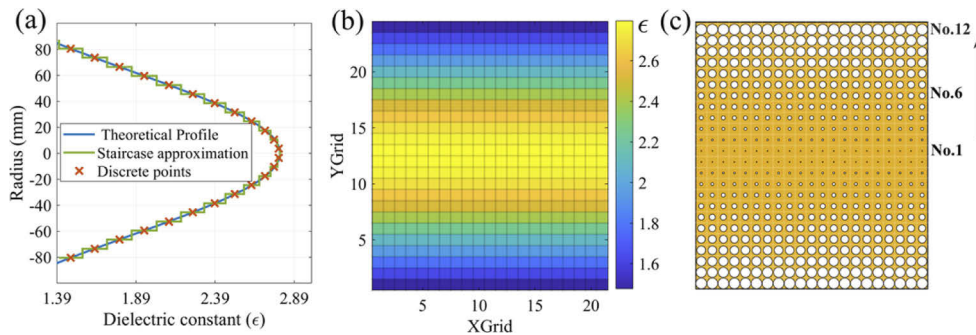
Fig. 3. (a) Staircase approximation of continuous relative permittivity profile of Mikaelian lens. (b) Discretization of 2-D relative permittivity profile (c) 2-D perforated structure of Mikaelian lens (24 layers).

Table 1. The air hole sizes for different layers of Mikaelian lens

Layer Number	Diameter of air hole (mm)
No.1	0.512
No.2	1.136
No.3	1.818
No.4	2.494
No.5	3.150
No.6	3.778
No.7	4.373
No.8	4.932
No.9	5.451
No.10	5.931
No.11	6.370
No.12	6.500

## 2.3. Ray tracing and beam-steering capability

To illustrate the beam-steering performance of ideal Mikaelian lens, a ray tracing algorithm based on above-mentioned ray transfer matrices is applied. Considering that the proposed lens is axially symmetric, Figs. 4(a), (d), (g) and (j) only give four examples of ray trajectory inside lens. The steering angles of beam is 0^0, 10^0, 20^0 and 35^0 respectively in these cases. Here, in order to further evaluate the steering capability of proposed lens with air-hole structure, a single patch antenna operating at 10 GHz is placed at the different positions of focal plane ($x = 0$mm, 10mm, 21mm, 40mm). The corresponding simulated 2-D electric field distribution is respectively shown in Figs. 4(b), (e), (h) and (k) by using the electromagnetic field full-wave simulation in CST Microwave Studio. Obviously, the results of these two methods are in reasonable agreement, which indicates the good phase transform function of lens converting a spherical wave into a plane wave. Figures 4(c), (f), (i) and (l) illustrate the different 3-D radiation patterns in different directions can be realized by selecting different feed positions at the focal plane of lens. It is to be noted that the loss tangent of lens material is not considered temporarily in this section.

However, it does not mean that the proposed lens can achieve the maximum steering angle of $\pm 35^0$ in practical application of antenna engineering. For beam-steering application, the feeding source need to be displaced from the focal point on the central axis to produce an off-axis beam. But it leads to various types of lens aberration including spherical aberration, coma, astigmatism, curvature of field, and distortion. Among these aberrations, the coma aberration is the most undesirable effect that causes severe asymmetrical side lobe distortion [20].

The design of proposed lens is based on above-mentioned ray tracing theory. The paraxial approximation is a key prerequisite in the design theory, which allows an important approximation: $\theta \approx \sin\theta \approx \tan\theta$. Thus, as can be seen from the Fig. 4(a), (d), (g) and (j), comatic aberration shows obvious increase as the off-axis angle of beam increases. It means that higher steering angles lead to higher phase error and deterioration of the corresponding radiated beam. Although the scan (gain) loss is about ~3dB with steering angel up to $\pm 35°$, the side-lobe level (SLL) is not much lower, as shown in Fig. 5.

2.4. Beam-switching concept for 1-D beam steerable lens antenna

The schematic view of proposed lens antenna excited by five rectangular microstrip patch antennas placed at the focal plane of lens is shown in Fig. 6. Different beam steering angles can be achieved by simply switching on or off different patch antennas. It should be noted that the patch
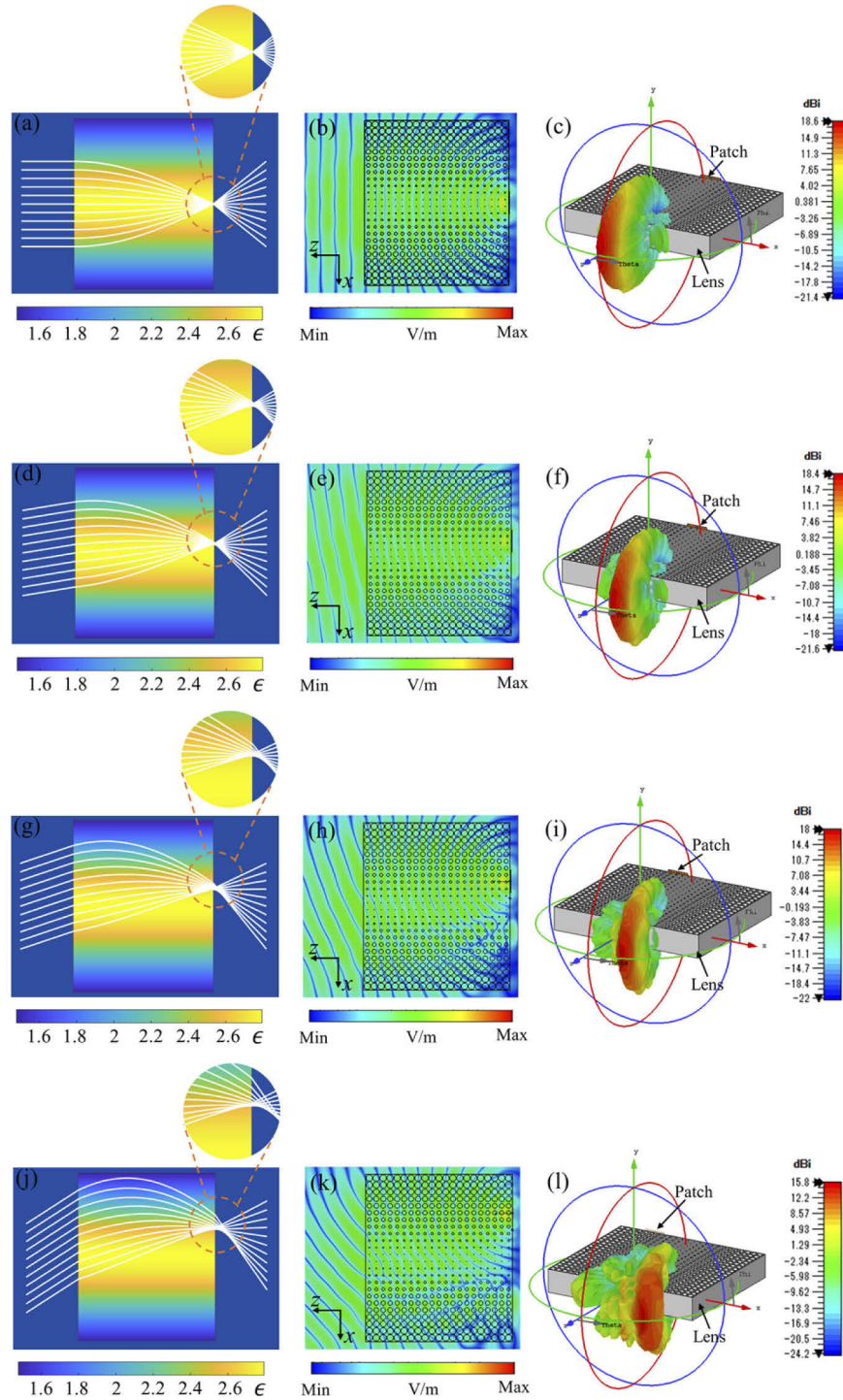
Fig. 4. Ray tracing analysis of ideal Mikaelian lens for different steering angles. (a) 0^0. (d) 10^0. (g) 20^0. (j) 35^0. Corresponding simulated 2-D electric field distribution for different feed positions. (b) $x = 0$ mm (e) $x = 10$ mm (h) $x = 21$ mm (k) $x = 40$ mm. The different 3-D radiation patterns in different directions (c) 0^0. (f) 10^0. (i) 20^0. (l) 35^0.
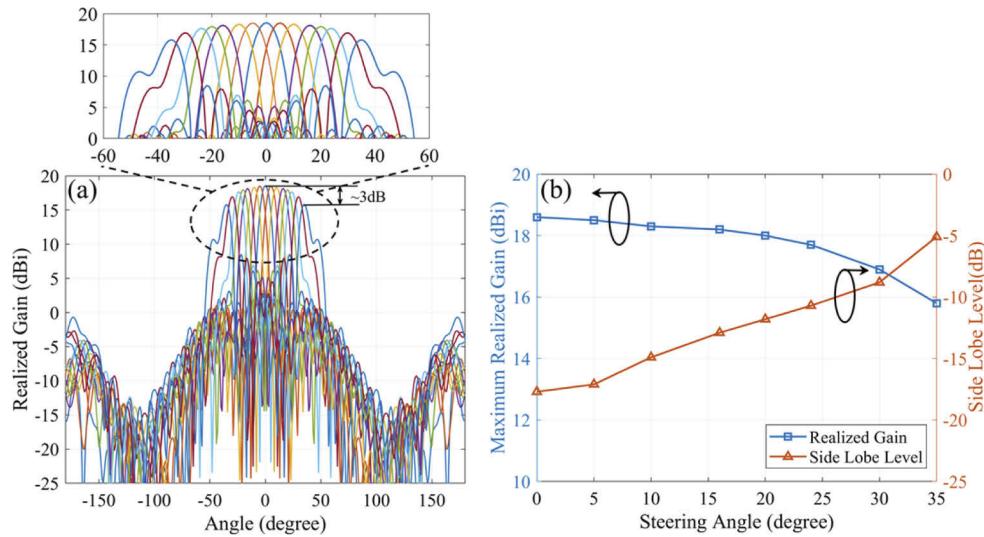
Fig. 5. (a) Simulated H-plane (xoz plane) radiation patterns for different feeding source positions of proposed lens operating at 10 GHz. (b) Simulated maximum realized gain and SLL versus steering angle.

spacing (*d*) is equal to 21 mm for reducing the mutual coupling (MC) between two microstrip patch antenna elements.

Table 2 lists the specific design parameters of lens antenna structure. The patch antenna is etched on the dielectric substrate with a relative permittivity of 2.55, loss tangent 0.001 and a thickness of 0.6 mm. And the polarization of the patch antenna is linear in z_0-axis direction. The lens focuses the radiation of patch antennas, which allows for beam-steering in the $x_0 o y_0$ plane. Each position on the focal plane of lens corresponds to the radiation in one defined direction. In our case, the pitch, length, width and thickness of proposed lens is 0.25, 168.8mm, 147.8mm and 25mm respectively.

Table 2. Geometry dimensions of Mikaelian lens antenna structure

Element	Parameter	Values (mm)
Lens	Length *l*	168.8
	Thickness *h*	25
	Width *w*	147.8
Patch	Patch_length *p_l*	8.56
	Patch_width *p_w*	11.25
	Patch_spacing *d*	21
Feed line	Feed_line_length *f_l*	5.16
	Feed_line_width *f_w*	1.68
Ground plane	Group_plane_length *gp_l*	25.68
	Group_plane_width *gp_w*	22.50
Matching line	Matching_line_width *ml_w*	1.1
	Matching_line_length *ml_l*	5.35
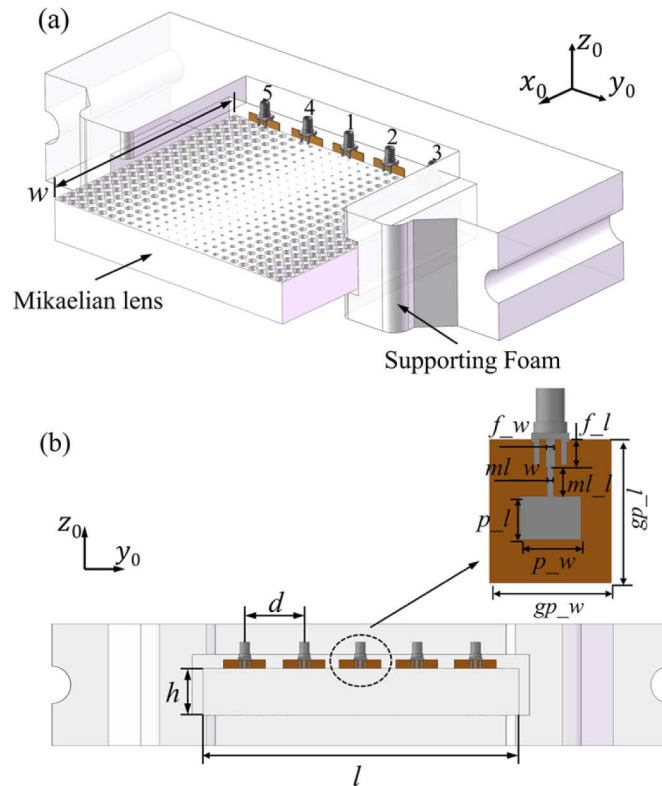
Fig. 6. Schematic of proposed Mikaelian lens antenna excited by five rectangular microstrip patch antennas in a 3-D model. (a) Perspective view. (b) Front view.

3. Measurement results and discussion

3.1. Prototype fabrications

A prototype of the proposed perforated Mikaelian lens with a total of 21×24 holes (minimum hole diameter 0.51mm) has been fabricated using SLA 3D printing (dimensional accuracy 0.1mm). Here, the SLA resin (C-UV 9400E) is utilized to construct the lens, which has a relative dielectric constant ~2.8, and loss tangent $\tan \delta \approx 0.02$[21]. Five patch antennas are glued to the rear surface of lens with equal distance of 21mm. Figure 7 shows the fabricated prototype of the Mikaelian lens antenna.

3.2. Experimental results

The measured reflection coefficient magnitude for each port is given respectively in Fig. 8(a). In our case, the common patch antennas operating at 10 GHz are utilized to be the feeding antenna, which has intrinsic limitations such as narrow bandwidth and low gain. Hence, the measured -10 dB impedance bandwidth is given instead of gain bandwidth. The measured -10 dB impedance bandwidth is about ~4%, which is limited by the feeding source (microstrip patch antenna). The frequency shift can be observed from the measured results, which could be attributed mainly to the presence of the perforated lens structure. It means that the certain amount of the frequency shift should be related to the equivalent permittivity for different air hole sizes where the patch antenna is placed. Besides, because of the limitation of 3-D printing, the phenomenon of warping or shrinkage would be observed that leads to unsmooth surface. The air gaps between patch antenna and lens caused by the unsmooth lens surface and gluing process
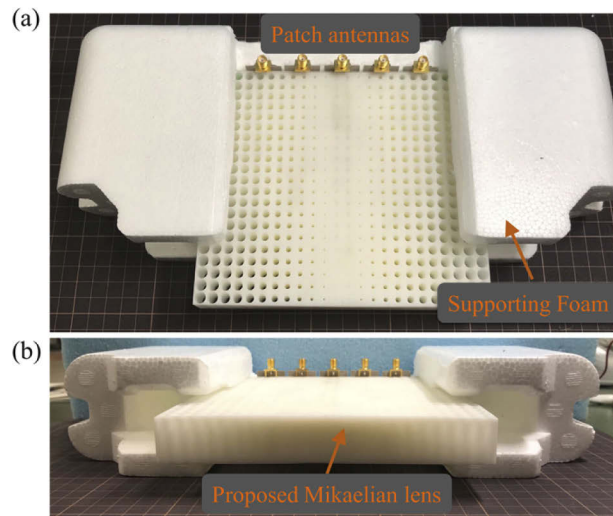
Fig. 7. Photographs of the fabricated Mikaelian lens antenna prototype. (a) Perspective view. (b) Front view.

a small impact on on the reflection coefficient magnitude. For coupling between these patch antennas, the coupling coefficients magnitude are shown in Fig. 8(b). The suitable patch spacing ($d = 21mm$) is selected to make the coupling coefficients magnitude less than -30 dB.
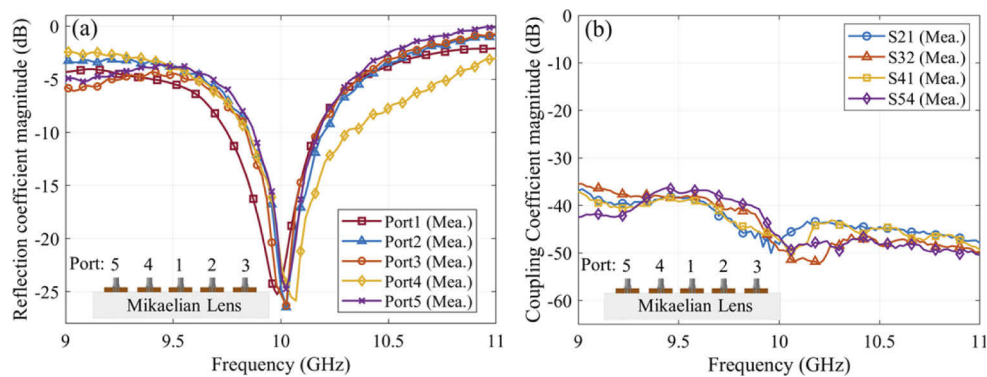

Fig. 8. (a) Measured reflection coefficient magnitude of proposed lens antenna for each port. (b) Measured coupling coefficients magnitude.

In our case, the measured center frequency of 10GHz is used for the experimental characterization of the radiation performances of proposed lens antenna. Considering that the proposed lens is axially symmetric, the measured normalized H-plane radiation pattern of the lens antenna at three feeding status are respectively illustrated for brevity in Fig. 9, which indicate that we can achieve beam-steering capabilities from $-20°$ to $+20°$ with around 13.2 dBi of realized gain and side-lobe levels (less than -11.5dB), and up to potential steering angles ($\pm30°$) with around 10 dBi of gain, by simply switching on or off different patch antennas. It is to be noted that the values of realized gain, HPBW, SLL and steering angles for different feeding status are all measured results. The complete set of measured H-plane radiation patterns for five different ports is shown in Fig. 10.
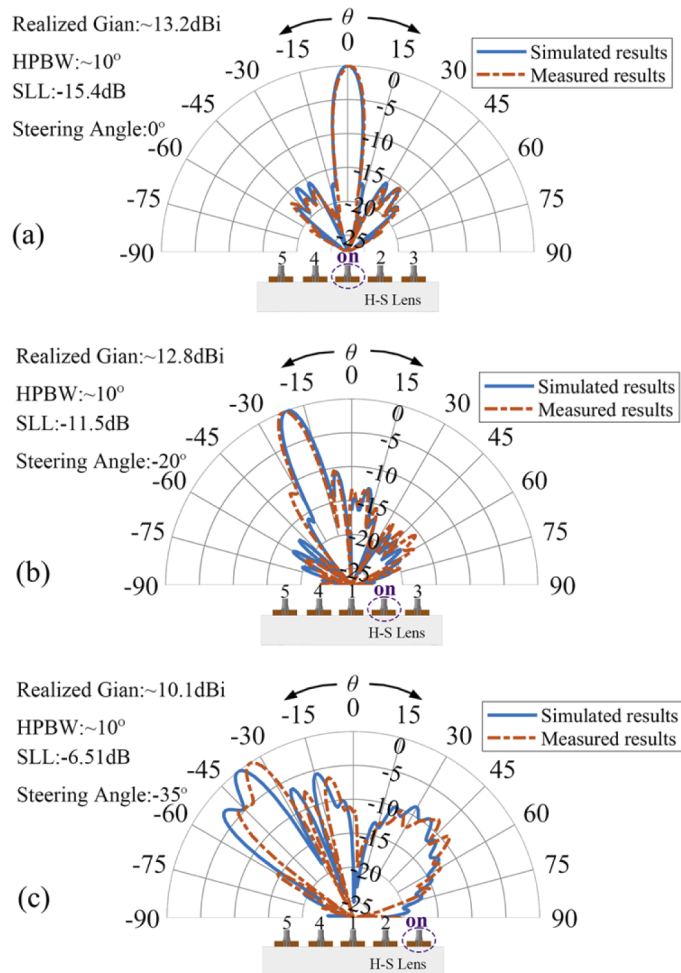
Fig. 9. Comparison between simulated and measured normalized H-plane radiation patterns at 10 GHz for different feeding status. (a) Port 1 on. (b) Port 2 on. (c) Port 3 on. Noted that the values of realized gain, HPBW, SLL and steering angles for different feeding status are all measured results.
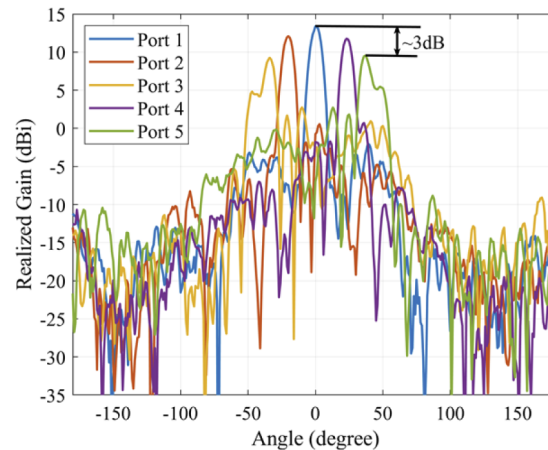
Fig. 10. Complete set of measured H-plane radiation patterns at 10 GHz for different port status.

3.3. Limitation and discussion

When the steering angel is up to ±35°, the side-lobe level deteriorates further, and could be considered not acceptable (−6.51dB). This phenomenon occurs mainly due to the intrinsic phase error of lens (comatic aberration) resulting from displacement of the feeding source from the focal point on the central axis, as described in Section 2.3. Moreover, although the SLA 3D printing is more accurate than FDM (fused deposition modeling), the loss tangent of SLA resin used in our case is higher compared to the commonly used materials such as PLA (∼0.011 at 10GHz) for FDM. Considering the loss tangent of SLA resin, the measured maximum realized gains with different steering angles are much lower than their simulated ones with lossless material (simulation in Section 2.3). Here, for the sake of brevity, the performance degradation for only feeding port 1 in the realized gain, total radiation efficiency, and SLL due to the high loss tangent is shown in Fig. 11(a), and (b) respectively. It means that the performance of proposed lens antenna can be further improved by using other materials with lower loss tangent. Besides, the total radiation efficiency is calculated by the following equation

$$\eta = G_e \lambda^2 / (4\pi A), \tag{6}$$

where G_e is the realized gain, A is the physical aperture size of the lens and λ is the wavelength at the designed frequency. The physical aperture size of proposed lens is little larger, considering that the common patch antenna at 10 GHz is utilized as feeding antenna. The aperture size can be further optimized to get good radiation efficiency. If the feed antenna with a higher directivity, the unwanted backside radiations would be suppressed, which can also improve the radiation performance.

Furthermore, the radiation performance of the lens system is both determined by the lens and the feeding antenna. The common patch antenna is utilized as feeding source in our cases, which has some drawbacks such as narrow-band. Thus, the proposed beam-switching lens antenna is also narrow-band. Despite the imperfections of the radiation performance (e.g., high side-lobe levels) with high steering angles and above-mentioned limitations, the simulation results are almost consistent with the measurement results considering uncertainties due to fabrication and measurement, as shown in Fig. 9. This proposed lens concept could be applied in the beam-steering applications for allowing a low-cost, low-profile and easy-to-fabricate beam-switching planar array antenna for microwave communication systems.
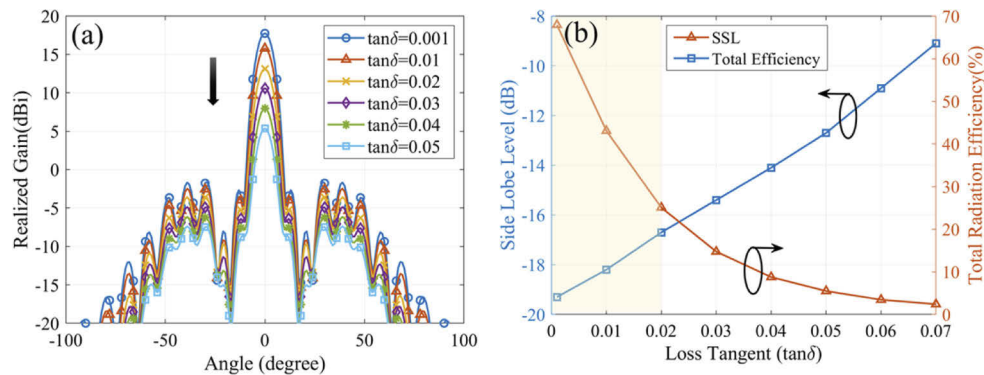
Fig. 11. The performance degradation for feeding port 1 in the gain, total efficiency, and SLL due to the loss of material. (a) Simulated H-plane radiation pattern at 10 GHz versus loss tangent (b) SLL and total radiation efficiency versus loss tangent respectively.

4. Conclusions

In this paper, the performance of an all-dielectric planar Mikaelian lens for 1-D beam-steering application was investigated. This new lens concept has its intrinsic flat shape characteristic, which allows for a simple low-cost planar feed technology. Based on ray tracing analysis and full-wave electromagnetic simulation, the performance of proposed lens prototype excited by five rectangular microstrip patch has been evaluated at 10 GHz. The simulated and measured results showed good agreement, demonstrating that we can achieve beam-steering capabilities in H planes from $-20°$ to $+20°$ with around 13.2 dBi of realized gain and SLL (less than -11.5dB), and up to $\pm30°$ with around 10 dBi of realized gain. Moreover, higher steering angles lead to higher phase error resulting from comatic aberration and deterioration of the corresponding radiated beam. Most importantly, the realized gain, efficiency and SLL can be further improved to get better radiation performances by using other 3-D printing materials with lower loss tangent or more advanced manufacturing technology. Due to its intrinsic flat shape characteristic, this proposed lens concept could be a potential alternative design for developing a low-cost, low profile and easy-to-fabricate beam-switching array antenna for microwave communication applications.

Disclosures. The authors declare no conflicts of interest.

Data availability. Data underlying the results presented in this paper are not publicly available at this time but may be obtained from the authors upon reasonable request.

References

1. T. S. Rappaport, Y. Xing, G. R. Maccartney, A. F. Molisch, E. Mellios, and J. Zhang, "Overview of millimeter wave communications for fifthgeneration (5G) wireless networks–with a focus on propagation models," IEEE Trans. Antennas Propag. **65**(12), 6213–6230 (2017).
2. R. J. Mailloux, Phased Array Antenna Handbook. (Artech House, 2005).
3. G. Washington, H. S. Yoon, M. Angelino, and W. H. Theunissen, "Design, modeling, and optimization of mechanically reconfigurable aperture antennas," IEEE Trans. Antennas Propag. **50**(5), 628–637 (2002).
4. J. R. Costa and C. A. Fernandes, "Broadband Slot Feed for Integrated Lens Antennas," Antennas Wirel. Propag. Lett. **6**, 396–400 (2007).
5. Q. Cheng, M. Naeem, and Y. Hao, "Composite Luneburg lens based on dielectric or plasmonic scatterers," Opt. Express **27**(8), 10946–10960 (2019).
6. Y. Li and Q. Zhu, "Luneburg lens with extended flat focal surface for electronic scan applications," Opt. Express **24**(7), 7201–7211 (2016).
7. H. D. Lu, Z. P. Liu, Y. B. Zhang, K. Pang, and Y. Liu, "Partial Maxwell fish-eye lens inspired by the Gutman lens and Eaton lens for wide-angle beam scanning," Opt. Express **29**(15), 24194–24209 (2021).

8. D. Headland, M. Fujita, and T. Nagatsuma, "Half-Maxwell fisheye lens with photonic crystal waveguide for the integration of terahertz optics," Opt. Express **28**(2), 2366–2380 (2020).

9. P. Bantavis, C. G. Gonzalez, R. Sauleau, G. Goussetis, S. Tubau, and H. Legay, "Broadband graded index Gutman lens with a wide field of view utilizing artificial dielectrics: a design methodology," Opt. Express **28**(10), 14648–14661 (2020).

10. G. Du, M. Liang, R. A. S. Garcia, C. Liu, and H. Xin, "3-D Printing Implementation of an X-band Eaton Lens for Beam Deflection," Antennas Wirel. Propag. Lett. **15**, 1487–1490 (2016).

11. M. Ebrahimpouri and O. Q. Teruel, "Bespoke Lenses Based on Quasi-Conformal Transformation Optics Technique," IEEE Trans. Antennas Propag. **65**(5), 2256–2264 (2017).

12. J. G. Marin and J. Hesselbarth, "Lens Antenna with Planar Focal Surface for Wide-Angle Beam-Steering Application," IEEE Trans. Antennas Propag. **67**(4), 2757–2762 (2019).

13. J. Bor, B. Fuchs, O. Lafond, and M. Himdi, "Flat foam-based Mikaelian lens antenna for millimeter wave applications," in *44th European Microwave Conference* (2014), pp. 1640–1643.

14. J. W. Yang, W. Y. Lai, H. C. Chou, and M. N. M. Kehn, "Compact Mikaelian Lens Synthesized by Metasurfaces," Antennas Wirel. Propag. Lett. **17**(3), 397–400 (2018).

15. J. Chen, H. C. Chu, Y. Lai, Z. Liu, H. Chen, M. Chen, and D. Fang, "Conformally Mapped Mikaelian Lens for Broadband Achromatic High Resolution Focusing," Laser Photonics Rev. **15**(5), 2000564 (2021).

16. F. Maggiorelli, A. Paraskevopoulos, J. C. Vardaxoglou, M. Albani, and S. Maci, "Profile Inversion and Closed Form Formulation of Compact GRIN Lenses," IEEE Open J. Antennas Propag. **2**, 315–325 (2021).

17. W. Y. Shao, H. Sato, X. T. Li, K. K. Mutai, and Q. Chen, "Perforated extensible 3-D hyperbolic secant lens antenna for directive antenna applications using additive manufacturing," Opt. Express **29**(12), 18932–18949 (2021).

18. A. Mikaelian and A. Prokhorov, "V Self-Focusing Media with Variable Index of Refraction," Prog. Opt. **17**, 279–345 (1980).

19. C. M. Segura, A. Dyke, H. Dyke, S. Haq, and Y. Hao, "Flat Luneburg Lens via Transformation Optics for Directive Antenna Applications," IEEE Trans. Antennas Propag. **62**(4), 1945–1953 (2014).

20. Y. T. Lo and S. W. Lee, "P Antenna Handbook: theory, applications, and design," Springer, 16–19 (2013).

21. S. Sahin, N. K. Nahar, and K. Sertel, "Dielectric properties of low-loss polymers for mmW and THz applications," J. Infrared, Millimeter, Terahertz Waves **40**(5), 557–573 (2019).